Title: The Cr dependent ion irradiation hardening in FeCrAl ODS steels with high Al concentration

Authors: Zhexian Zhang[1*], Siwei Chen[1,2], Kiyohiro Yabuuchi[1], Peng Dou[3], Akihiko Kimura[1,3]

Affiliations:

1. Institute of Advanced Energy, Kyoto University, Gokasho, Uji, Kyoto, 611-0011, Japan

2. Department of Nuclear Engineering, University of Tennessee, Knoxville, TN 37996, USA

3. School of Materials Science and Engineering, Chongqing University, Chongqing, 400044, China

Corresponding Author:

Zhexian ZHANG

Email address: zx-zhang@iae.kyoto-u.ac.jp

Coauthors:

Siwei CHEN: schen83@utk.edu

Kiyohiro YABUUCHI: yabuuchi.kiyohiro.7e@kyoto-u.ac.jp

Peng DOU: doup@cqu.edu.cn

Akihiko KIMURA: kimura@iae.kyoto-u.ac.jp

Abstract

The FeCrAl ODS steels for accident tolerant fuel claddings are designed with concentration limitation of Al. In this study, we investigated the FeCrAl ODS steels with 9wt% Al, which is close to the up-limit of Al concentration. Particularly, we studied the Cr dependence on the self-ion irradiation hardening in these steels. Three ODS steels, Fe12Cr9Al (SP12), Fe15Cr9Al (SP13), and Fe18Cr9Al (SP14) were irradiated with 6.4MeV Fe^{3+} at 300 °C to nominal 3 dpa. The irradiation hardening was investigated by nanoindentation, and the Nix-Gao method was used to evaluate the bulk-equivalent hardness. The results showed that the irradiation hardening will decrease with increased Cr concentration, where Fe18Cr9Al had significant smaller hardening than the Fe12Cr9Al and Fe15Cr9Al ODS steels. TEM observation showed both <100> and ½<111> dislocation loops existed in the irradiated area. The irradiation hardening was estimated by dispersed barrier hardening (DBH) model with dislocation loops. This research could fill the gaps of irradiation effects in high-Al FeCrAl ODS steels.

Keyword

FeCrAl ODS steels, self-ion irradiation, Nano-indentation, irradiation hardening, High Al FeCrAl steels

1. Introduction

Accident tolerant fuel (ATF) cladding has been proposed to enhance the safety of light water reactors (LWR) under design-basis and beyond-design-basis accident scenarios, aiming to delay the onset of detrimental oxidation and chemical interaction processes, reduce the reaction heat, lower the temperature rise, and resultantly minimize the potential for off-site radioactive releases[1,2]. The FeCrAl ODS steels are considered as the most promising candidate with both the excellent mechanical properties and good oxidation resistance at high temperatures[3–5]. During operation, the FeCrAl claddings will experience neutron irradiation at operating temperature around 280 to 300°C, which induces generation of defects such as dislocation loops, voids, precipitates and so on. These defects will lead to irradiation embrittlement, for example, shift the ductile brittle transition temperature (DBTT) greatly over room temperature[6]. This degradation could be reflected by the irradiation hardening that the higher yielding stress usually indicates lower ductility after irradiation[7]. Therefore, it is important to understand the materials' hardening behavior under irradiation in similar reactor environments.

The FeCrAl ODS steels are designed with different Cr (<~20wt%) and Al (<~10wt%) concentrations. The up-limit of Cr is due to the α-α′ phase separation during thermal aging at elevated temperatures through spinodal and nucleation-growth mechanism according to the miscibility gap[8,9]. On the other hand, the Al concentration is limited to below 10wt%. The reason is above this concentration, Fe-Al precipitates will appear in aging and even during fabrication[10]. High Al will also induce the formation of Al-Ti enriched β′ precipitates, which causes embrittlement during early aging at 475°C[11,12].

So far, the irradiation investigations in FeCrAl ODS steels are mainly focused on materials with Al less than 9wt%[13–19]. However, high Al could shift the miscibility boundary of α-α′ phase separation to a higher Cr concentration[8,20], consequently hinders the α′ precipitation hardening. Moreover, corrosion tests showed small amount of Al (2~4wt%) could efficiently reduce the weight gains in supercritical pressurized water (SCPW) [21]. With these merits of Al, it is important to understand the material behavior with high Al concentration close to its up-limit.

Another issue in FeCrAl alloys is the Cr dependent irradiation hardening. The alloy element Cr will improve the corrosion resistance by forming protective Cr_2O_3 layers. However, the irradiation embrittlement could be accelerated by the α-α′ separation with increased Cr as well as radiation enhanced diffusion[22]. The α′ precipitation in FeCrAl steels has been studied and proved susceptible to composite concentrations[23], temperature[24] and grain morphology[25,26], and the precipitate kinetics under irradiation follows typical Lifshitz-Slyozov-Wagner (LSW) theory[27]. Both the ion-irradiation and neutron irradiation showed Cr-dependence on irradiation hardening in FeCrAl steels[28,29].

To fill the gap of research in high-Al FeCrAl ODS steels, we investigated the FeCrAl ODS ferritic steels with 9wt% Al which is close to its up-limit. Particularly to understand the Cr-dependent irradiation hardening, the steels with different concentration of Cr (12, 15, 18wt%) were studied. These steels were subjected to self-ion irradiation to nominal 3 dpa at 300°C. The hardness of steels was measured by nanoindentation, and microstructures were observed by TEM. The Cr dependent hardening in FeCrAl ODS steels with high Al concentrations was discussed.

2. Experimental

Three SP-series FeCrAl ODS ferritic steels, of which the chemical compositions are shown in Table 1. These steels were produced by mechanical alloying in Ar atmosphere. The mixed powder was encapsulated into a steel capsule, hot-extruded at 1150°C and followed by the final step of a heat treatment at 1150°C for 1hr and air cooling. The producing procedure could be found in a recent review[30]. Specimens for irradiation were cut along the extrusion direction, grinded with SiC paper and polished with 3μm, 1μm, 0.25μm diamond powders subsequently. Final surface treatment included electrical polishing in 5% $HClO_4$ and 95% CH_3COOH for 60 sec, and low-energy Ar ion milling for 10 min.

Ion irradiation was performed with Dual-beam Facility for Energy Science and Technology (DuET) in Kyoto University. DuET is composed of a 1.7 MV tandem accelerator for heavy ion irradiation and a 1.0MV single accelerator for helium implantation. Details of the construction can be found in Ref[31]. The ion source of Fe_2O_3 was ionized by an 860 ionizer in

Cesium reservoir. The ionized charged particle, FeO^-, was focused by Einzel lens and deflected by an injector magnet to accelerator. In the tandem accelerator, the FeO^- beam was first accelerated to 1.7 MeV halfway, then stripped into 1.32 MeV Fe^{3+} and 0.38 MeV oxygen ions. The Fe^{3+} was accelerated again in the other half of the accelerator with the total energy of Fe^{3+} becoming 6.4MeV. A magnet accelerator was used thereafter to screen out ions other than 6.4 MeV Fe^{3+}. Beam position was finally adjusted by a steerer, and beam current was measured by array of 21 Faraday cups. The vacuum of the target chamber was 5×10^{-5} Pa. The beam irradiated on specimen was raster-scanned horizontally 1000 Hz and vertically 300 Hz. The temperature of irradiated sample surface was monitored by infrared thermography during irradiation. The emissivity of materials was calculated by pre-calibration with a K-type thermocouple attached to the specimen surface at various temperatures before irradiation.

Table 1. Chemical compositions of FeCrAl ODS ferritic steels (wt%, Bal. Fe).

	ID	Cr	Al	Ti	Y	C	O	N	Ar
Fe12Cr9Al	SP12	11.93	8.65	0.53	0.38	0.029	0.22	0.003	0.006
Fe15Cr9Al	SP13	14.25	8.4	0.51	0.38	0.03	0.22	0.003	0.006
Fe18Cr9Al	SP14	16.63	8.09	0.49	0.37	0.032	0.22	0.003	0.006

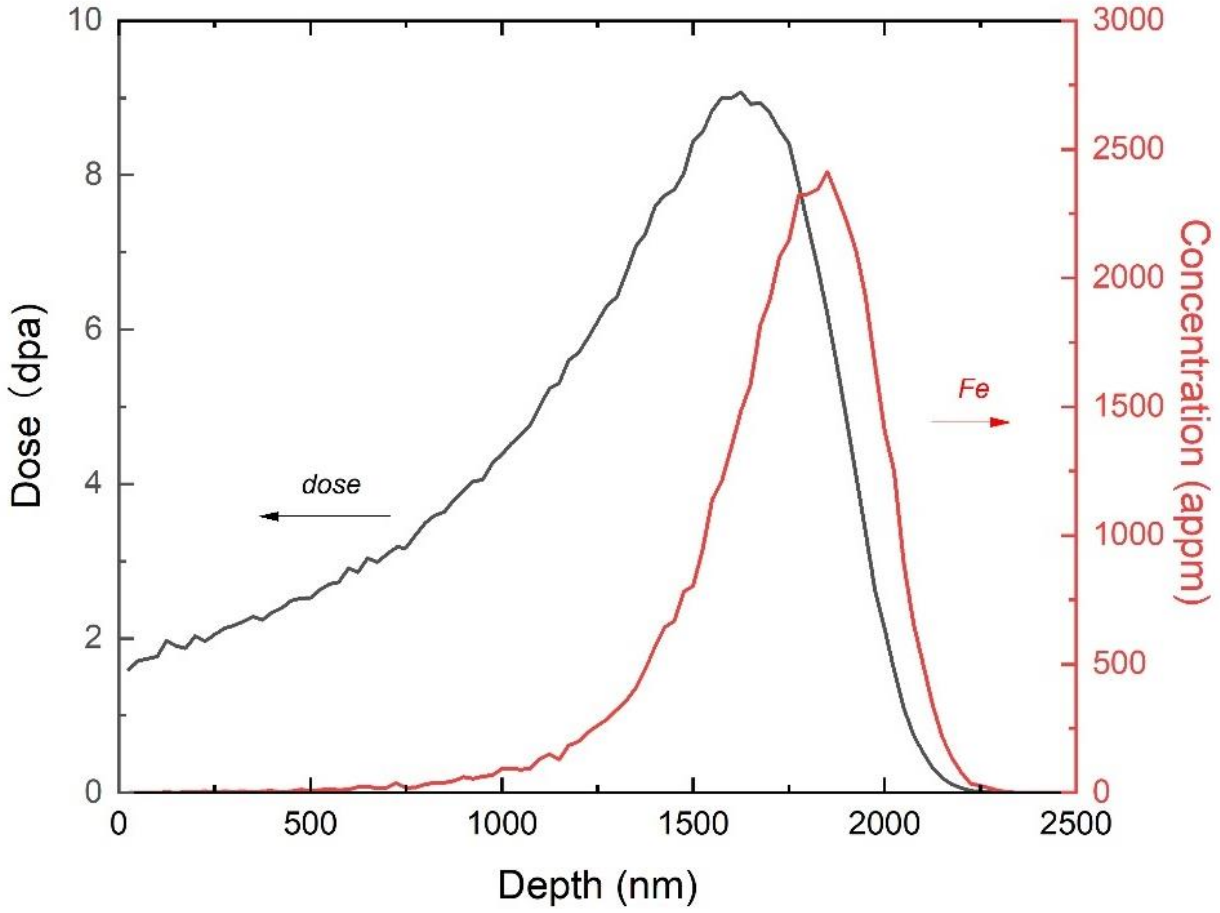

Figure 1. Irradiation dose and implanted Fe ions distribution calculated by SRIM. 3dpa at 600 nm was selected as a nominal value.

The irradiation damage and implanted ion distribution (Fig.1) were estimated by SRIM[32] using the "Ion distribution and quick calculation of damage" method. The displacement threshold energy(TDE) was selected by 40 eV[33] for iron-based steels. The value at the depth of 600 nm was chosen as the nominal irradiation dose because there is barely interference of the implanted irons at this range. The samples were irradiated to nominal 3 dpa at 300 °C with the beam flux of 1.1×10^{12} ions/cm^2/s, which is corresponding to 3.3×10^{-4} dpa/s. The peak dose is located around 1.6 μm. The maximum damage distribution is about 2.3 μm.

Nano-hardness was measured by G200 nanoindentation with a Berkovich tip using continuous stiffness measurement (CSM) method. The oscillation amplitude was 2 nm, and the frequency was 45 Hz. The strain rate is constant 0.05 s^{-1}, which was achieved by loading rate control[34]. The area function was calibrated on fused silica (E=72.0GPa, ν=0.17). Over 20 tests were performed on each sample. The tests were indented to maximum 2 μm depth and held for 10s at the max loading.

Tensile tests were performed on the tensile machine (INTESCO Co., Ltd) with a load cell of 0.5 kN. The geometries of a dog-born sheet type of miniature tensile specimens measured gauge-length=5 mm, width=1.2 mm and thickness=0.25 mm with the gripping area on both sides of 4×4mm^2. The displacement speed was 0.2 mm/min resulting in an initial strain rate of 6.67×10^{-4} /s. The yield stress was defined as 0.2% off-set flow stress. Three tests for each material were done at room temperature. Micro-Vickers hardness was tested by HMV-2T (Shimadzu Corp.) with 2 kg load and holding time for 10 sec. Both the tensile and hardness tests were performed at room temperature.

Microstructures of specimens were observed by Jeol 2010 TEM with a side-mount CCD camera. The cross-section of irradiated specimens was fabricated by focused ion beam machining (FIB, Hitachi FB2200). TEM specimens were flashing-polished in 5% $HClO_4$ and 95% CH_3OH at -30 °C and 30 V as final thinning. The images were taken under two-beam bright field condition, with (110) αFe diffraction plane excited. The thickness of TEM specimens was measured by extinction fringes along specimen margins or inclined non-twinned large angle grain boundaries under g3g weak beam central dark field condition.

3. Results

3.1. The oxide morphology and mechanical properties before irradiation

The oxides in Al-added FeCrAl ODS steels are mainly Y-Al-O types. The lattice image analysis by Oono et al showed most of the oxides were $Y_4Al_2O_9$ (YAP) and $YAlO_3$ (YAM)[35]. The morphology of dispersoids before irradiation were shown in Fig.2. Both dislocation lines and oxides exist in the materials. The dislocations are straight lines, indicating the tension along the dislocation curves are fully relieved in the heat treatment after mechanical alloying. Some

interactions between dislocation lines and oxides can be observed but still, there are no curved dislocation lines around oxide particles.

Fig. 3 shows the size distribution of oxide particle diameters in the three as-received FeCrAl ODS steels. The diameters are mainly between 4~8 nm, which means the size of oxides are generally homogeneous. The average diameter of the oxides tends to increase with decreasing Cr concentration. The Fe18Cr9Al has the highest number densities of oxides in three steels. The estimated volume fractions are 0.51%, 0.62% and 0.64% for Fe12Cr9Al, Fe15Cr9Al, and Fe18Cr9Al, respectively.

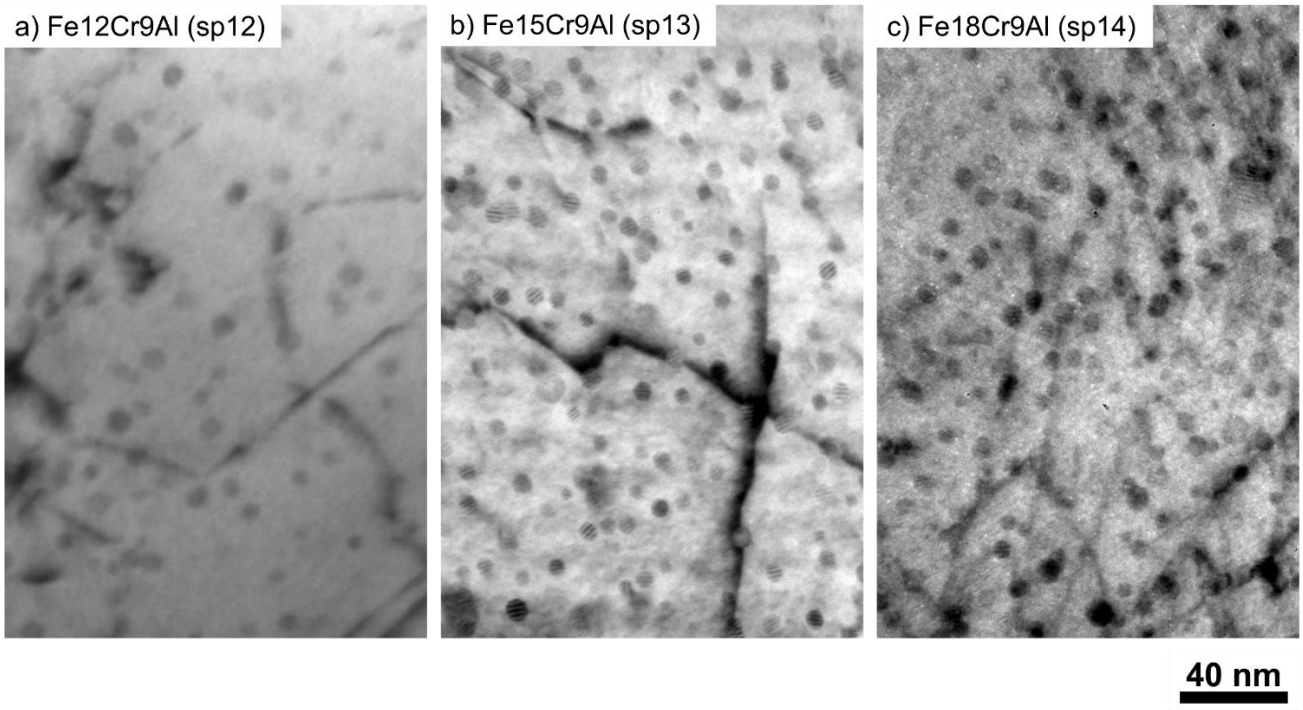

Figure 2. The oxides morphology in a) Fe12Cr9Al, b) Fe15Cr9Al, c) Fe18Cr9Al ODS steels before irradiation.

The bulk equivalent hardness from nanoindentation tests were estimated by Nix-Gao model[36] in equation (1), where H is the measured hardness, H_0 is the bulk equivalent hardness, h^* is a length scale indicator, h is the indentation depth.

$$H^2 = H_0^2\left(1 + {}^{h^*}/_{h}\right) \quad (1)$$

Bulk-equivalent nano-hardness of unirradiated materials were estimated by data between 100 to 2000nm. Relationships among nano-hardness (NH), Vickers hardness (HV) and yielding stress (YS, $\sigma_{0.2}$) were shown in Fig.4. The NH=0.01346HV is similar to the previous obtained results[37]. However, the YS=2.764HV is different to the common acknowledged 3 times rules[38].

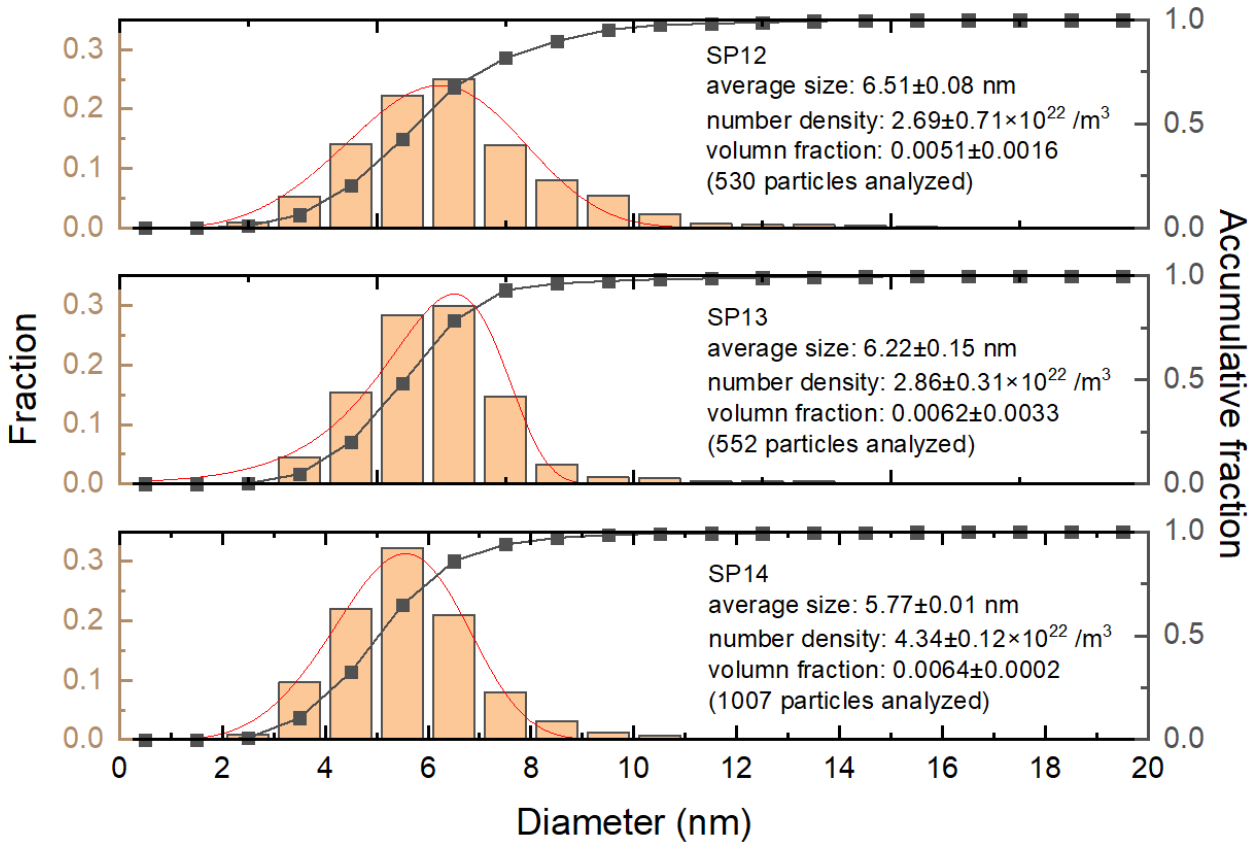

Figure 3. The size distribution of oxides in unirradiated Fe12Cr9Al (SP12), Fe15Cr9Al (SP13), and Fe18Cr9Al (SP14) ODS steels. The red lines are fitted results by Weibull distribution. The volume fractions were obtained by an average of observed three areas.

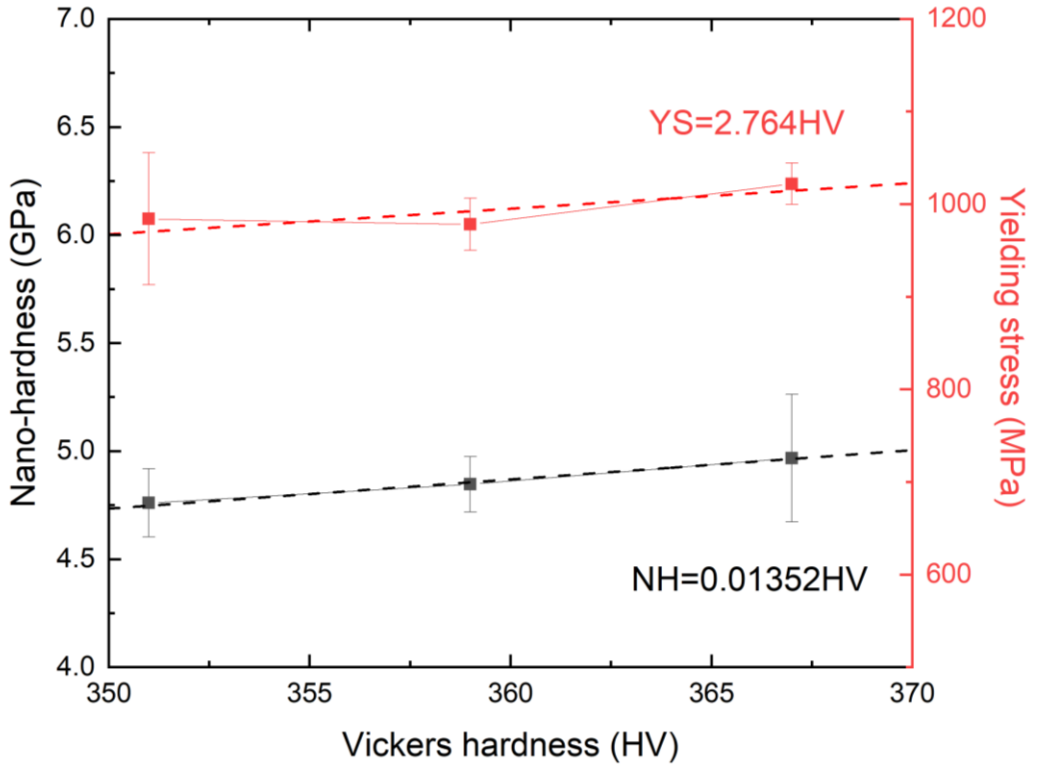

Figure 4. The relationship between nano-hardness (NH), Vickers hardness (HV) and $\sigma_{0.2}$ yielding stress (YS) in the three ODS ferritic steels before irradiation. The nano hardness was obtained by Nix-Gao methods. The intercept was preset as zero for linear fitting.

3.2. The microstructure evolution after irradiation

Fig.5 shows the cross-section of irradiation damaged Fe12Cr9Al (SP12). The overall damaged region was compared to the SRIM calculated dose profile (Fig.5a). The dislocation loops distributed to maximum 1.8 μm, which exceeded the damage peak calculated by SRIM, but was shallower than the maximum distribution range. Fig.5b shows the microstructures in the region between 150~770 nm, which was selected as the area for TEM analysis. In this region, dislocation loops coexisted with oxide particles and dislocation lines. Fig.5c shows the transition area of the irradiated region. In this region, dislocation loops disappeared and only dislocation lines and oxides existed in the unirradiated area.

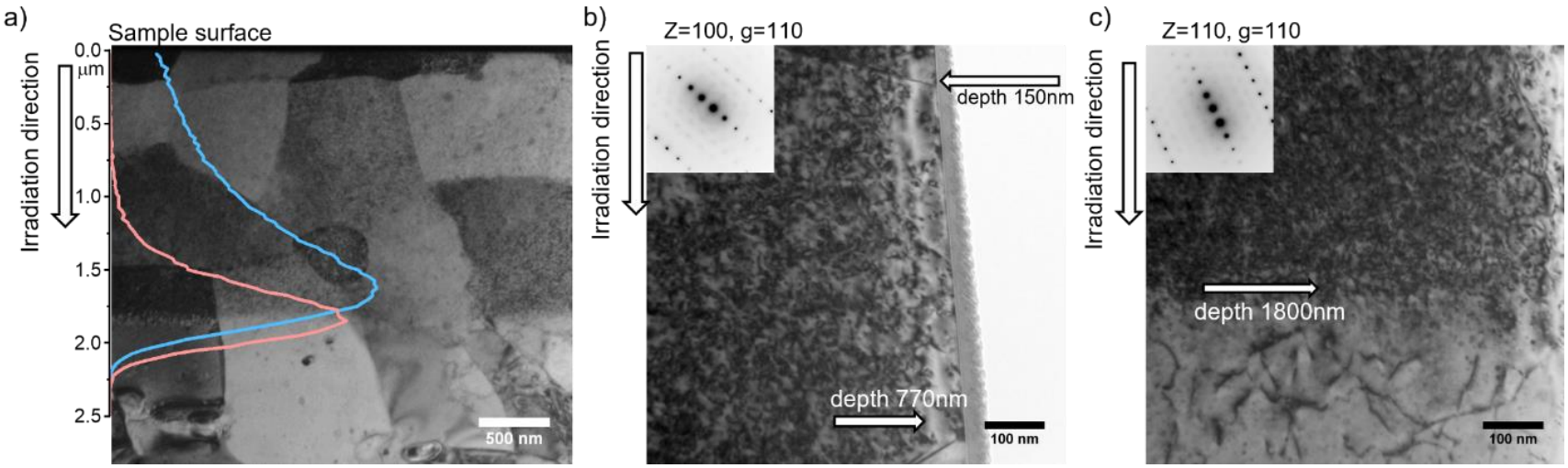

Figure 5. Microstructures of irradiated Fe12Cr9Al ODS steels (SP12). a) the overall distribution, the morphology of dislocation loops in the region b) between irradiation depth of 150nm~770nm, c) at the transition area

Fig. 6 shows two different areas around 600 nm depth of the irradiated Fe15Cr9Al (SP13) under zone axis [011] and [133], with *g* vectors equals to -200 and 01-1 respectively. The projection of ½<111> and <100> dislocation loops with different habit planes under different zone axis were calculated. The solid circles are the loops appearing with contrast and the dashed circles are the loops being extinct at this diffraction condition. Both Fig. 6a and Fig. 6b proved the existence of the ½<111> and <100> type dislocation loops and the oxide particles in the irradiated region. The Moiré fringes indicated that the oxides were not amorphized. The diffraction patterns in Fig.6c and Fig.6d showed that the oxides were mainly YAP, with αFe(0-11) corresponding to YAP(221) because they have similar plane spacing. Fig6c also showed another relationship of αFe(001)//YAP(1-20) and αFe[100]//YAP[210].

Song et al[39] studied the stability of oxide particles in ODS steels under ion-irradiation at 200 °C based on the observation of Moiré fringes, and reported that the Y-Al-O oxides tended to become amorphous under irradiation up to ~8 dpa and dissolved thereafter. They suggested that the radiation tolerance of the oxide particles depended on both the irradiation temperature and damage rate as well as total damage (dpa). In this study, under the ion-irradiation at 300 °C and almost the same damage rate, the oxides were not amorphized, which means the Y-Al-O system oxides are relatively stable at this irradiation condition. It might be also owing to the smaller dose used in this experiment compared to the study of Song et al[39].

The average diameter and number density of dislocation loops were summarized in Table 2, where the density of dislocation loops was adjusted according to the invisible criterion in TEM two beam diffraction condition. The diameters of dislocation loops in SP12 and SP13 are 11.6±2.0nm and 12.0±1.0nm, and the number densities are $2.26\pm0.34\times10^{22}/m^3$ and $1.84\pm0.85\times10^{22}/m^3$, respectively.

Table 2. The dislocation loops and DBH hardening after irradiation.

	Dislocation loops		Hardening (GPa)	
	Diameter(nm)	Density($\times10^{22}/m^3$)	Measured	Calculated
Fe12Cr9Al(SP12)	11.6±2.0	2.26±0.34	1.45±0.27	1.28
Fe15Cr9Al(SP13)	12.0±1.0	1.84±0.85	1.35±0.33	1.18

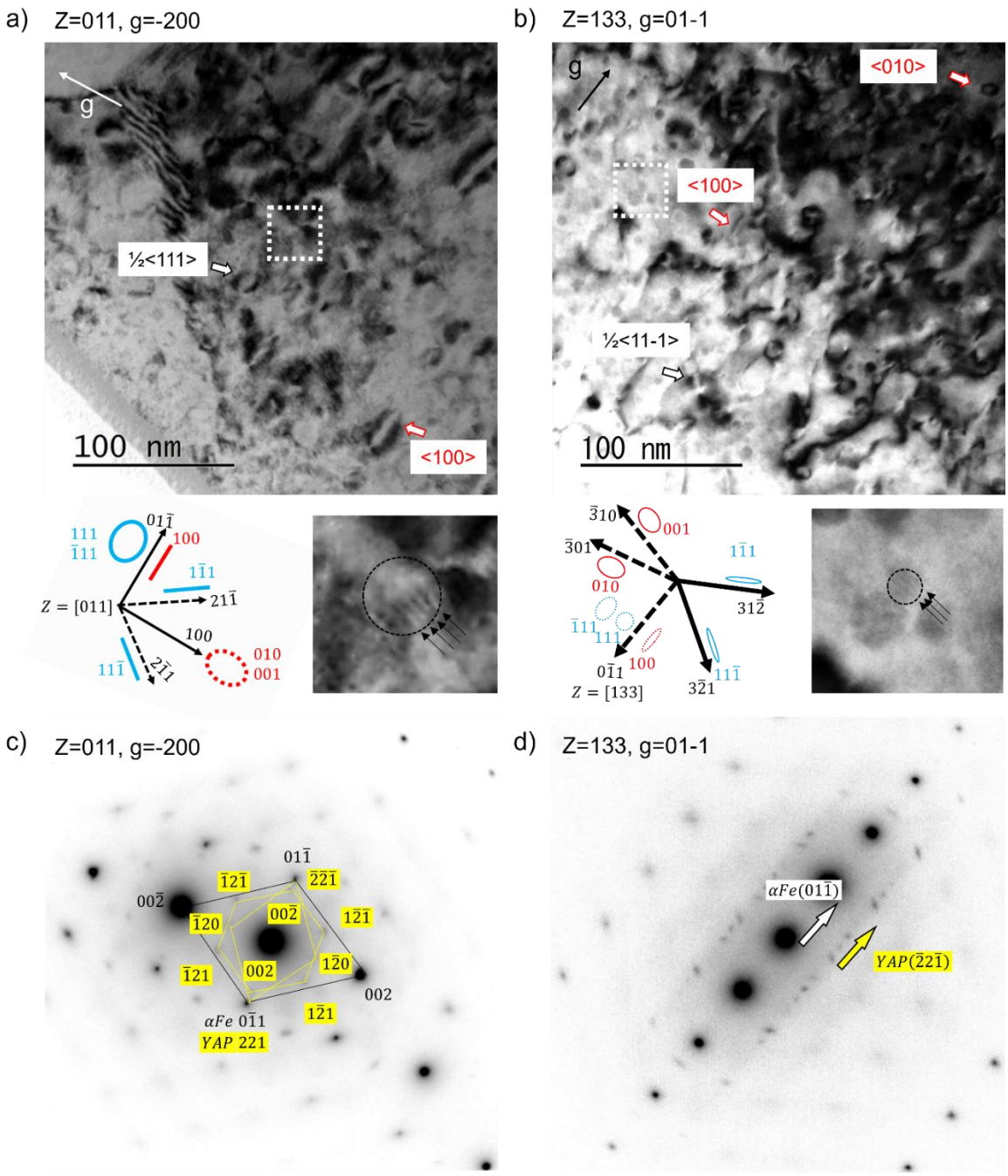

Figure 6. Microstructures of irradiated Fe15Cr9Al ODS steel (SP13), a) g=200, b) g=110. Dislocation loops projections were shown in each zone axis. The Moiré fringes of oxides indicate crystal structure was kept under irradiation. The diffraction pattern of the irradiated area along c) [011] direction and d) [133] direction.

The average diameter and number density of dislocation loops were summarized in Table 2, where the density of dislocation loops was adjusted according to the invisible criterion in TEM two beam diffraction condition. The diameters of dislocation loops in SP12 and SP13 are 11.6±2.0nm and 12.0±1.0nm, and the number densities are $2.26\pm0.34\times10^{22}/m^3$ and $1.84\pm0.85\times10^{22}/m^3$, respectively.

Table 2. The dislocation loops and DBH hardening after irradiation.

	Dislocation loops		Hardening (GPa)	
	Diameter(nm)	Density($\times10^{22}/m^3$)	Measured	Calculated
Fe12Cr9Al(SP12)	11.6±2.0	2.26±0.34	1.45±0.27	1.28
Fe15Cr9Al(SP13)	12.0±1.0	1.84±0.85	1.35±0.33	1.18

3.3. The nano-indentation hardness

The profiles of nanoindentation hardness of irradiated and unirradiated FeCrAl ODS steels are shown in Fig.7. The features of the profiles include: 1) the hardness decreases gradually along with depth because of size effect, 2) a reverse size effect in some tests before ~100nm occurred possibly because of initial contact variance from surface roughness, grain boundaries and precipitates, but as the indent went deeper, the normal size effect became dominant. 3) the irradiated samples have elevated hardness than the unirradiated ones indicating irradiation hardening. 4) the hardening disappeared at an indentation depth around 2000 nm where the plastic deformation zone in the irradiated region took small fraction compared to the unirradiated region.

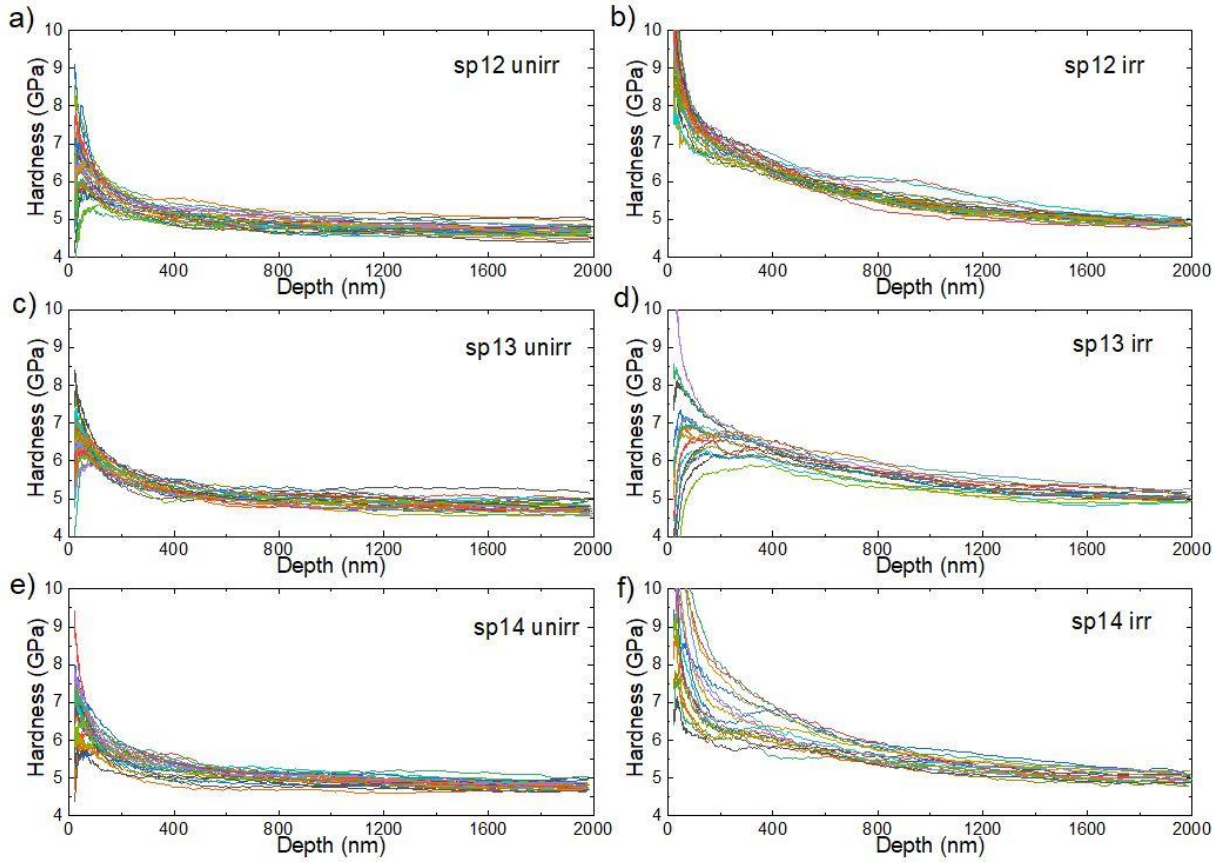

Figure 7. The nano-indentation hardness profile of a) unirradiated and b) irradiated Fe12Cr9Al (SP12), c) unirradiated and d) irradiated Fe15Cr9Al (SP13), e) unirradiated and f) irradiated Fe18Cr9Al (SP14).

The Nix-Gao hardness plots of both irradiated and unirradiated steels are shown in Fig.8. Before irradiation, the Nix-Gao plots were linear through the entire exhibited range. In contrast, there is a clear shoulder of irradiated plots in the depth region lower than 300 nm, which reflects the plastic region in damaged area. The bulk-equivalent hardness was estimated by the linear fitting of the data between 100 nm~2000 nm in the unirradiated specimens. The irradiated hardness was evaluated by data with different ranges between 100 nm~350 nm of Nix-Gao plots. The depth of damage limit at 1800 nm corresponds to about 5 times of the turning point at 350 nm.

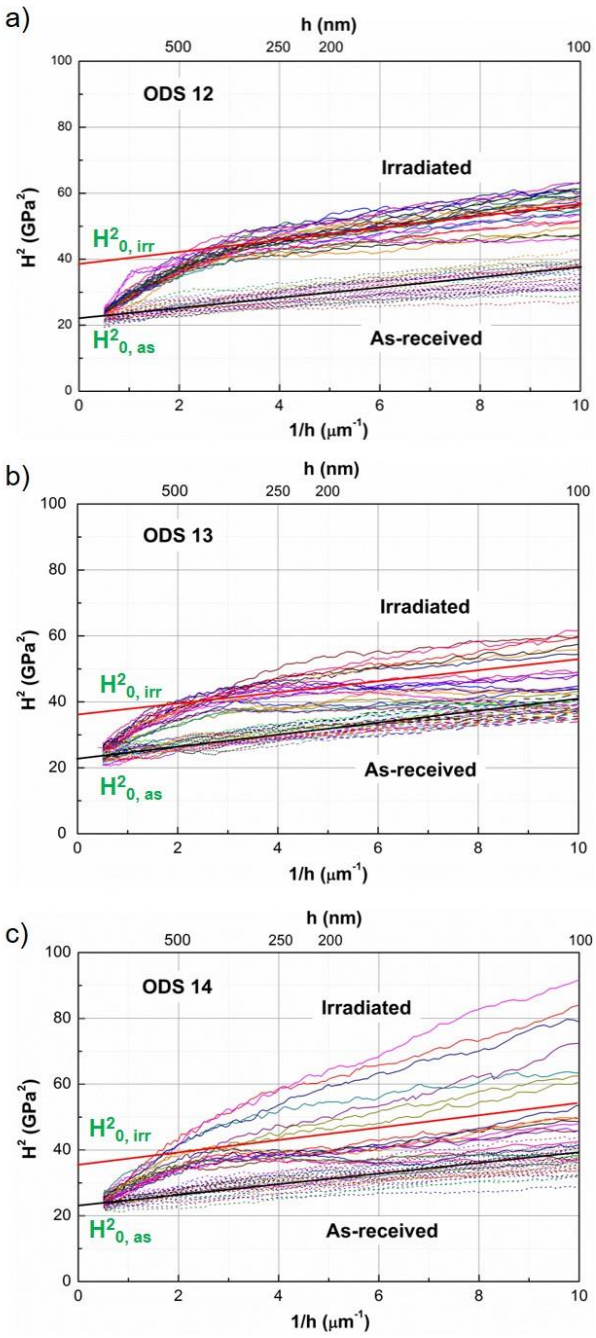

Figure 8. Nix-Gao plots of the irradiated and unirradiated a) Fe12Cr9Al ODS steel (SP12), b) Fe15Cr9Al ODS steel (SP12) and c) Fe18Cr9Al ODS steel (SP14). Note that the manually drawn lines are only an indicator to the shoulder for linear fitting and do not correspond to the actual bulk equivalent hardness.

The depth range selection for hardness evaluation of irradiation is not only dependent on the linear correlation. This is because the profile of Nix-Gao plots is usually not absolutely linear[40]. Moreover, the surface roughness[41] and pile up[42] will affect the measured hardness not only increasing scattering but change the linear relationship. The bulk-equivalent nano-hardness evaluated by different range of Nix-Gao plots were summarized in Table 3. For Fe12Cr9Al and Fe15Cr9Al, as the selected range goes deeper, the evaluated hardness keeps decreasing. Oppositely, the evaluated hardness of Fe18Cr9Al increases with selected depth until around 6 GPa. These are typical phenomenon in irradiated materials, where the surfaces are inhomogeneous either because of irradiation induced defects or roughness.

Table 3. The bulk-equivalent nano-hardness (GPa) evaluated by different range of Nix-Gao plots.

Range of Nix-Gao plots	Fe12Cr9Al (SP12) irradiated	Fe15Cr9Al (SP13) irradiated	Fe18Cr9Al (SP14) irradiated
100nm – 250nm	6.23±0.27	6.22±0.35	5.72±0.31
100nm – 300nm	6.21±0.23	6.19±0.31	5.80±0.26
100nm – 350nm	6.16±0.21	6.16±0.27	5.83±5.83
150nm – 250nm	6.22±0.29	6.14±0.38	5.95±0.32
200nm – 300nm	6.12±0.28	6.08±0.27	6.02±0.38
200nm – 350nm	5.97±0.29	6.04±0.30	5.95±0.43

In this study, we chose the 100nm-300nm as the standard range to evaluate bulk-hardness for irradiated materials, because in this range, the indentation deforming zone is fully within the irradiated region. Fig.9 summarized the bulk-equivalent hardness of each nanoindentation of the irradiated and unirradiated steels. In unirradiated steels, the hardness linearly increases with Cr concentration. In irradiated materials, Fe12Cr9Al and Fe15Cr9Al showed similar high hardness while Fe18Cr9Al had the lowest.

4. Discussion

Figure 10 summarized the irradiation hardening in several FeCrAl ODS and non-ODS steels at similar irradiation conditions[13,15,24,28,43]. In this study, the irradiation hardening exhibited Cr dependence, where higher Cr yielded smaller irradiation hardening. However, this

trend is contradicted to the conventional understanding that high Cr should generate more α′ precipitate, thus yield a higher irradiation hardening. This trend is also opposite to the hardening of FeCrAl non-ODS steels which were subjected to neutron irradiation reported by Field et al[28] (Fig.10). There is a small successive decrease of the Al concentration in the studied steels (Table 1), which might affect the formation of Al-enrich β′ precipitates, and consistent with the decreasing trend of irradiation hardening. However, the effect is doubtful because of the tiny difference of the Al concentrations (<1%). Future works may require APT characterization of the α′ and β′ to understand the precipitation hardening under self-ion irradiations.

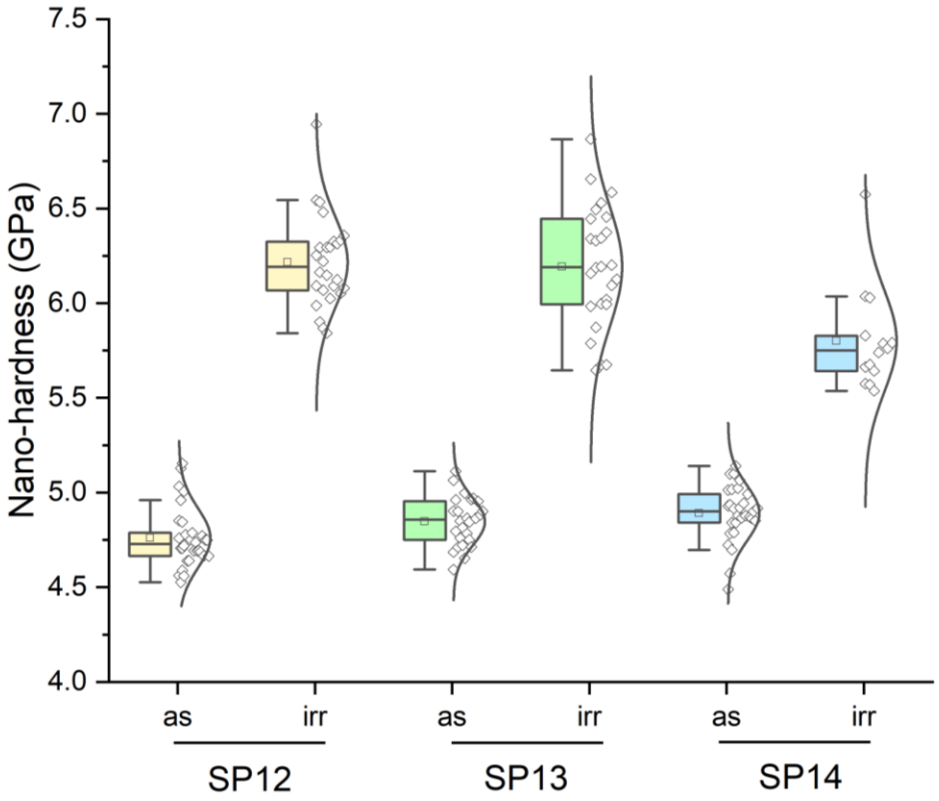

Figure 9. The bulk-equivalent hardness calculated by Nix-Gao method with the data from 100nm to 1000nm of the unirradiated and from 100nm to 300nm of the irradiated materials.

The solution atoms of Cr could play an essential role in the evolution of dislocation loops under irradiations[26]. Firstly, the solute element Cr could impede the growth of dislocation loops. This effect will make loops grow into small sizes with high densities. Secondly, the Cr will hinder the migration of ½<111> loops. The formation of <100> loops by two glissile

½<111> reaction will be suppressed[44], and the sessile <100> loops are considered as stronger obstacles for dislocation migration than ½<111> loops. Thirdly, the formation energy of <100> loops is much larger than ½<111> loops, and the energy increasing much faster with Cr concentration in <100> loops than the latter. Thus, the irradiation hardening will be reduced by suppressing formation of <100> loops with elevated Cr concentrations.

The examination of the dislocation loops was performed in Fe12Cr9Al and Fe15Cr9Al ODS steels. As the samples are limited, only the information of total dislocation loops was compared (Table 2). Generally, the dislocation loops in Fe12Cr9Al are slightly smaller and denser than in Fe15Cr9Cr ODS steels, which is consistent with the above analysis.

The simplified dispersed barrier hardening (DBH) model (equation 2) is used to evaluate the hardening induced by dislocation loops. In equation (2), M=3.06 is the Taylor factor for FCC and BCC materials. The coefficient α=0.2 is a strength factor. The shear modulus μ is 82 GPa for FeCrAl ODS steels. The Burgers vector b is 0.249 nm for glissile ½<111> dislocation. N and d present for the number density and diameter of loops, respectively.

$$\Delta\sigma_{loop} = M\alpha\mu b\sqrt{Nd} \qquad (2)$$

The estimated hardening by dislocation loops for SP12 and SP13 are 1.28 GPa and 1.18 GPa respectively. The measured hardening by nanoindentation were 1.45±0.27 GPa and 1.35± 0.33 GPa for SP12 and SP13 (Table 2).

Other factors which may influence the hardening are defect sink position including grain boundaries, pre-existed dislocations, and oxides. In the solid-solution strengthening analysis by Ukai et al[45], the grain sizes of the same SP-series steels are measured the same, and the dislocation densities are considered similar. Here we follow the same assumption. The oxides, however, may contribute to the differences. On one hand, the surface of oxides are effective annihilation sites for point defects such as interstitials and vacancies. On the other hand, atoms in large oxides may subject to knock-out effects, dissolute into matrix and reprecipitate as satellite clusters around original oxide[15]. This progress can explain the decreasing trend of hardening, with the increased number density of oxides, which offered larger surface area in total, and decreased diameter, which reduced the possibility of dissolution (Fig.3).

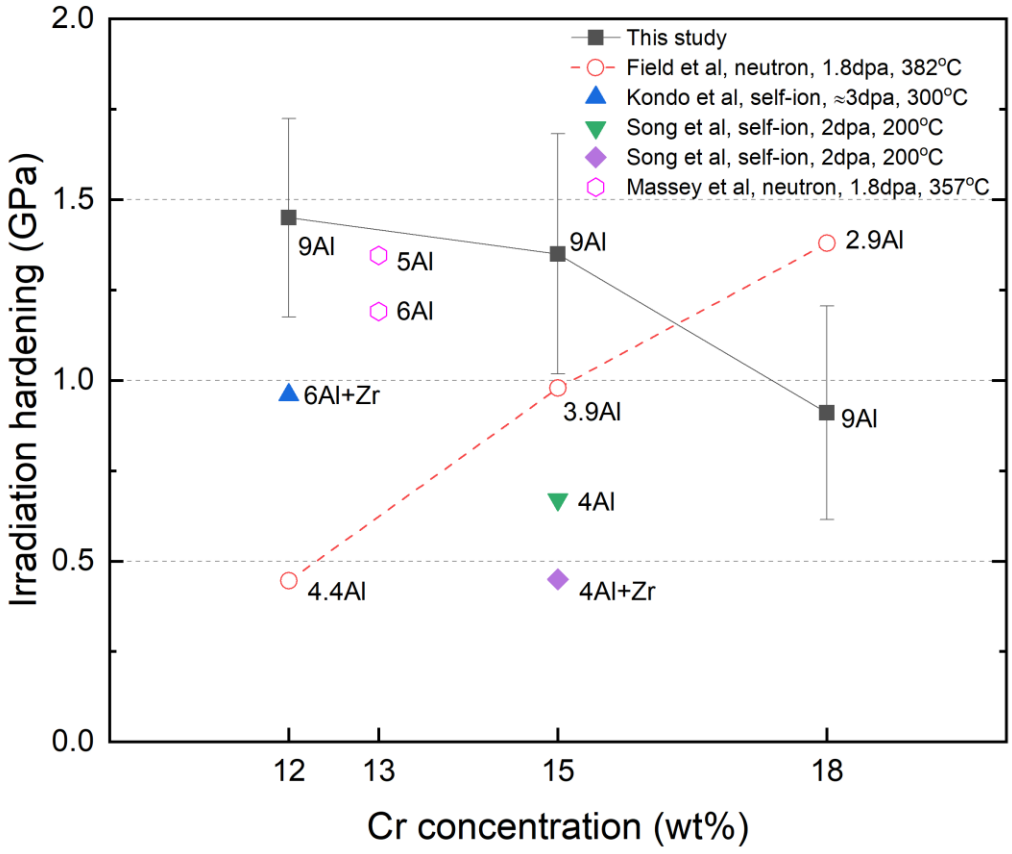

Figure 10. The summary of Cr dependent irradiation hardening in FeCrAl steels. The solid symbols stand for ODS steels, and hollow symbols are non-ODS steels. The neutron irradiation hardening measured by yield stress were converted to nanoindentation hardening by NH(GPa)=0.004891YS(MPa).

Moreover, it seems reducing Al and adding Zr will reduce the irradiation hardening, according to the hardening results from Kondo et al[13] and Song et al[15] (Fig.10). Although there are some differences in the irradiation condition in Fe15Cr4Al(Zr), with lower temperature (200°C) and damage dose (2dpa), the results are reasonable by the explanation that the oxide density is much higher in steels with 4wt%Al+Zr than with 9wt%Al, where irradiation defects were annihilated by the larger oxide surface area.

Lower irradiation hardening usually indicates better irradiation resistance, though it is not absolutely correct due to various assessment standards. The irradiation hardening results in this study suggest higher Cr (18wt%) might be a better option when Al reaches 9wt%. The current study in high Al FeCrAl steels will help to understand materials behavior at the irradiation conditions. It may contribute to the FeCrAl material design near the safe boundary of element concentration.

5. Summary

The Cr dependent irradiation hardening in FeCrAl ODS steels with high Al concentration was studied. Three FeCrAl ODS steels, Fe12Cr9Al (SP12), Fe15Cr9Al (SP13), and Fe18Cr9Al (SP14), were irradiated with 6.4MeV Fe^{3+} at 300 °C to nominal 3 dpa. Both ½<111> and <100> dislocation loops formed after irradiation. No void appeared in the irradiated region. Oxides remained crystalline after irradiation at experiment temperature. The irradiation hardening and microstructure evolution were investigated by nanoindentation. The hardening decreases with increasing Cr in 9wt%Al FeCrAl ODS steels. Particularly, the Fe18Cr9Al showed the lowest irradiation hardening in the experiment condition. The solute Cr atoms are considered to hinder the growth of dislocation loops and to suppress <100> loops formation, that reduced the irradiation hardening. Besides, oxides might also influence the hardening. The results will give reference for material design with high Al in FeCrAl ODS steels.

Acknowledgement

We gratefully acknowledge Prof. Kondo and Mr. Hashitomi for their helping with the ion irradiation in DuET, Kyoto University (Prof. Kondo has now migrated to Tohoku University). ZXZ acknowledges Prof. Stuart A. Maloy in Los Alamos National Laboratory for the discussion ATF element selection. ZXZ acknowledges Prof. Kasada in Tohoku University for discussion on nanoindentation.

References

[1] S.J. Zinkle, K.A. Terrani, J.C. Gehin, L.J. Ott, L.L. Snead, Accident tolerant fuels for LWRs: A perspective, Journal of Nuclear Materials. 448 (2014) 374–379.

[2] K.A. Terrani, Accident tolerant fuel cladding development: Promise, status, and challenges, Journal of Nuclear Materials. 501 (2018) 13–30.

[3] A. Kimura, S. Ukai, M. Fujiwara, Development of fuel clad materials for high burn-up operation of SCPR, Proc. GENES4/ANP2003, Paper. 1198 (2003).

[4] A. Kimura, R. Kasada, N. Iwata, H. Kishimoto, C. Zhang, J. Isselin, P. Dou, J. Lee, N. Muthukumar, T. Okuda, Super ODS steels R&D for fuel cladding of next generation nuclear systems 1) Introduction and alloy design, in: Atomic Energy Society of Japan, 2009: pp. 2187–2194.

[5] A. Kimura, R. Kasada, N. Iwata, H. Kishimoto, C. Zhang, J. Isselin, P. Dou, J. Lee, N. Muthukumar, T. Okuda, Development of Al added high-Cr ODS steels for fuel cladding of next generation nuclear systems, Journal of Nuclear Materials. 417 (2011) 176–179.

[6] S. Maloy, E. Aydogan, O. Anderoglu, C. Lavender, Y. Yamamoto, Viability of thin wall tube forming of ATF FeCrAl.; Los Alamos National Lab.(LANL), Los Alamos, NM (United States), Pacific Northwest National Lab.(PNNL), Richland, WA (United States). (2016).

[7] S.A. Maloy, T.A. Saleh, O. Anderoglu, T.J. Romero, G.R. Odette, T. Yamamoto, S. Li, J.I. Cole, R. Fielding, Characterization and comparative analysis of the tensile properties of five tempered martensitic steels and an oxide dispersion strengthened ferritic alloy irradiated at ≈295 °C to ≈6.5 dpa, Journal of Nuclear Materials. 468 (2016) 232–239. https://doi.org/10.1016/j.jnucmat.2015.07.039.

[8] S. Kobayashi, T. Takasugi, Mapping of 475 °c embrittlement in ferritic Fe-Cr-Al alloys, Scripta Materialia. 63 (2010) 1104–1107. https://doi.org/10.1016/j.scriptamat.2010.08.015.

[9] D. Chen, A. Kimura, W. Han, H. Je, Age-hardening susceptibility of high-Cr ODS ferritic steels and SUS430 ferritic steel, Fusion Engineering and Design. 98–99 (2015) 1945–1949. https://doi.org/10.1016/j.fusengdes.2015.05.078.

[10] B.C. Maji, S. Ukai, N. Oono-Hori, Microstructural stability and intermetallic embrittlement in high Al containing FeCrAl-ODS alloys, Materials Science and Engineering: A. 807 (2021) 140858. https://doi.org/10.1016/j.msea.2021.140858.

[11] W. Sang, P. Dou, A. Kimura, Early-stage thermal ageing behavior of 12Cr, 12Cr–7Al and 18Cr–9Al ODS steels, Journal of Nuclear Materials. 535 (2020) 152164. https://doi.org/10.1016/j.jnucmat.2020.152164.

[12] A. Kimura, W. Sang, W. Han, K. Yabuuchi, Z. Xin, J. Luan, P. Dou, Twofold age-hardening mechanism of Al-added high-Cr ODS ferritic steels, Journal of Nuclear Materials. 575 (2023) 154223.

[13] K. Kondo, S. Aoki, S. Yamashita, S. Ukai, K. Sakamoto, M. Hirai, A. Kimura, Ion irradiation effects on FeCrAl-ODS ferritic steel, Nuclear Materials and Energy. 15 (2018) 13–16. https://doi.org/10.1016/j.nme.2018.05.022.

[14] P. Song, D. Morrall, Z. Zhang, K. Yabuuchi, A. Kimura, Radiation response of ODS ferritic steels with different oxide particles under ion-irradiation at 550 C, Journal of Nuclear Materials. 502 (2018) 76–85.

[15] P. Song, K. Yabuuchi, P. Spätig, Insights into hardening, plastically deformed zone and geometrically necessary dislocations of two ion-irradiated FeCrAl (Zr)-ODS ferritic steels: A combined experimental and simulation study, Acta Materialia. 234 (2022) 117991.

[16] J. Gao, Y. Yamasaki, P. Song, Y.-J. Huang, K. Yabuuchi, A. Kimura, K. Sakamoto, S. Yamashita, Dose dependence of ion irradiation effects on 12Cr–6Al-ODS steel with electron-beam weld line, Journal of Nuclear Materials. 528 (2020) 151858.

[17] E. Getto, M. Johnson, M. Maughan, N. Nathan, J. McMahan, B. Baker, K. Knipling, S. Briggs, K. Hattar, M.J. Swenson, Friction stir welding and self-ion irradiation effects on microstructure and mechanical properties changes within oxide dispersion strengthened steel MA956, Journal of Nuclear Materials. 567 (2022) 153795. https://doi.org/10.1016/j.jnucmat.2022.153795.

[18] E. Getto, N. Nathan, J. McMahan, S. Taller, B. Baker, Understanding radiation effects in friction stir welded MA956 using ion irradiation and a rate theory model, Journal of Nuclear Materials. 561 (2022) 153530. https://doi.org/10.1016/j.jnucmat.2022.153530.

[19] X. Zhou, L. Guo, Y. Wei, H. Wang, C. Chen, Y. Chen, W. Zhang, S. Liu, R. Liu, S. Mo, Effect of aluminum content on dislocation loops in model FeCrAl alloys, Nuclear Materials and Energy. 21 (2019) 100718.

[20] J. Ejenstam, M. Thuvander, P. Olsson, F. Rave, P. Szakalos, Microstructural stability of Fe-Cr-Al alloys at 450-550 °C, Journal of Nuclear Materials. 457 (2015) 291–297. https://doi.org/10.1016/j.jnucmat.2014.11.101.

[21] A. Kimura, R. Kasada, N. Iwata, H. Kishimoto, C.H. Zhang, J. Isselin, P. Dou, J.H. Lee, N. Muthukumar, T. Okuda, M. Inoue, S. Ukai, S. Ohnuki, T. Fujisawa, T.F. Abe, Development of Al added high-Cr ODS steels for fuel cladding of next generation nuclear systems, Journal of Nuclear Materials. 417 (2011) 176–179. https://doi.org/10.1016/j.jnucmat.2010.12.300.

[22] E.R. Reese, N. Almirall, T. Yamamoto, S. Tumey, G. Robert Odette, E.A. Marquis, Dose rate dependence of Cr precipitation in an ion-irradiated Fe[sbnd]18Cr alloy, Scripta Materialia. 146 (2018) 213–217. https://doi.org/10.1016/j.scriptamat.2017.11.040.

[23] P.D. Edmondson, S.A. Briggs, Y.Yamamoto, R.H. Howard, K. Sridharan, K.A. Terrani, K.G. Field, Irradiation-enhanced α′ precipitation in model FeCrAl alloys, Scripta Materialia. 116 (2016) 112–116. https://doi.org/10.1016/j.scriptamat.2016.02.002.

[24] C.P. Massey, P.D. Edmondson, K.G. Field, D.T. Hoelzer, S.N. Dryepondt, K.A. Terrani, S.J. Zinkle, Post irradiation examination of nanoprecipitate stability and α′ precipitation in an oxide dispersion strengthened Fe-12Cr-5Al alloy, Scripta Materialia. 162 (2019) 94–98.

[25] D. Zhang, S.A. Briggs, P.D. Edmondson, M.N. Gussev, R.H. Howard, K.G. Field, Influence of welding and neutron irradiation on dislocation loop formation and α′ precipitation in a FeCrAl alloy, Journal of Nuclear Materials. 527 (2019) 151784.

[26] K.S. Mao, C.P. Massey, Y. Yamamoto, K.A. Unocic, M.N. Gussev, D. Zhang, S.A. Briggs, O. Karakoc, A.T. Nelson, K.G. Field, Improved irradiation resistance of accident-tolerant high-strength FeCrAl alloys with heterogeneous structures, Acta Materialia. 231 (2022) 117843.

[27] K.G. Field, K.C. Littrell, S.A. Briggs, Precipitation of α′ in neutron irradiated commercial FeCrAl alloys, Scripta Materialia. 142 (2018) 41–45.

[28] K.G. Field, X. Hu, K.C. Littrell, Y. Yamamoto, L.L. Snead, Radiation tolerance of neutron-irradiated model Fe–Cr–Al alloys, Journal of Nuclear Materials. 465 (2015) 746–755.

[29] E. Aydogan, J.S. Weaver, S.A. Maloy, O. El-Atwani, Y.Q. Wang, N.A. Mara, Microstructure and mechanical properties of FeCrAl alloys under heavy ion irradiations, Journal of Nuclear Materials. 503 (2018) 250–262.

[30] S. Ukai, K. Sakamoto, S. Ohtsuka, S. Yamashita, A. Kimura, Alloy Design and Characterization of a Recrystallized FeCrAl-ODS Cladding for Accident-Tolerant BWR Fuels: An Overview of Research Activity in Japan, Journal of Nuclear Materials. (2023) 154508.

[31] A. Kohyama, Y. Katoh, M. Ando, K. Jimbo, New Multiple Beams-Material Interaction Research Facility for radiation damage studies in fusion materials, Fusion Engineering and Design. 51–52 (2000) 789–795. https://doi.org/10.1016/S0920-3796(00)00181-2.

[32] J.F. Ziegler, M.D. Ziegler, J.P. Biersack, SRIM–The stopping and range of ions in matter (2010), Nuclear Instruments and Methods in Physics Research Section B: Beam Interactions with Materials and Atoms. 268 (2010) 1818–1823.

[33] N. Astm, Standard practice for neutron radiation damage simulation by charged-particle irradiation, Annu. B. ASTM Stand. 12 (1996) E521.

[34] B.N. Lucas, W.C. Oliver, Indentation power-law creep of high-purity indium, Metallurgical and Materials Transactions A. 30 (1999) 601–610.

[35] N.H. Oono, S. Ukai, S. Hayashi, S. Ohtsuka, T. Kaito, A. Kimura, T. Torimaru, K. Sakamoto, Growth of oxide particles in FeCrAl- oxide dispersion strengthened steels at high temperature, Journal of Nuclear Materials. 493 (2017) 180–188. https://doi.org/10.1016/j.jnucmat.2017.06.018.

[36] W.D. Nix, H. Gao, Indentation size effects in crystalline materials: a law for strain gradient plasticity, Journal of the Mechanics and Physics of Solids. 46 (1998) 411–425.

[37] K. Yabuuchi, Y. Kuribayashi, S. Nogami, R. Kasada, A. Hasegawa, Evaluation of irradiation hardening of proton irradiated stainless steels by nanoindentation, Journal of Nuclear Materials. 446 (2014) 142–147.

[38] J.T. Busby, M.C. Hash, G.S. Was, The relationship between hardness and yield stress in irradiated austenitic and ferritic steels, Journal of Nuclear Materials. 336 (2005) 267–278.

[39] P. Song, A. Kimura, K. Yabuuchi, P. Dou, H. Watanabe, J. Gao, Y.-J. Huang, Assessment of phase stability of oxide particles in different types of 15Cr-ODS ferritic steels under 6.4 MeV Fe ion irradiation at 200° C, Journal of Nuclear Materials. 529 (2020) 151953.

[40] P. Haušild, Methodological comment on the nanoindentation of ion-irradiation hardened materials, Journal of Nuclear Materials. 551 (2021) 152987.

[41] C. Walter, C. Mitterer, 3D versus 2D finite element simulation of the effect of surface roughness on nanoindentation of hard coatings, Surface and Coatings Technology. 203 (2009) 3286–3290.

[42] P. Zhu, Y. Zhao, S. Agarwal, J. Henry, S.J. Zinkle, Toward accurate evaluation of bulk hardness from nanoindentation testing at low indent depths, Materials & Design. 213 (2022) 110317.

[43] P. Song, J. Gao, K. Yabuuchi, A. Kimura, Ion-irradiation hardening accompanied by irradiation-induced dissolution of oxides in FeCr(Y, Ti)-ODS ferritic steel, Journal of Nuclear Materials. 511 (2018) 200–211. https://doi.org/10.1016/j.jnucmat.2018.09.007.

[44] J.C. Haley, S.A. Briggs, P.D. Edmondson, K. Sridharan, S.G. Roberts, S. Lozano-Perez, K.G. Field, Dislocation loop evolution during in-situ ion irradiation of model FeCrAl alloys, Acta Materialia. 136 (2017) 390–401. https://doi.org/10.1016/j.actamat.2017.07.011.

[45] S. Ukai, Y. Yano, T. Inoue, T. Sowa, Solid-solution strengthening by Al and Cr in FeCrAl oxide-dispersion-strengthened alloys, Materials Science and Engineering: A. 812 (2021) 141076. https://doi.org/10.1016/j.msea.2021.141076.